Research Article

Structural transformation and room temperature ammonia sensing properties of TiS_2 nanostructures

Shivani Sharma[1] · Sukhwinder Singh[1] · Ravi Chand Singh[1] · Sandeep Sharma[1]

Received: 17 January 2020 / Accepted: 30 March 2020 / Published online: 11 April 2020

Abstract
The nanostructures of TiS_2 have been successfully synthesized in a single-step process using probe sonication in various liquid media. Initial visual inspection confirmed that the nanostructures prepared in de-ionized water and de-ionized water–ethanol mixture change color from black to white with time. Various structural, optical and vibrational measurements identified these changes due to structural transformation of TiS_2 into TiO_2 in presence of water molecules. However, this transformation was absent in TiS_2 nanostructures prepared in media like di-methyle formamide and *N*-methyle pyrolidone. These nanostructures were used for making two terminal sensor devices and yielded entirely different results. The black colored TiS_2 showed highly selective n-type behaviour towards ammonia (200 ppm) with nearly 72% relative response at room temperature. Corresponding rise time and recovery time were found to be 72 ± 7 s and 165 ± 10 s, respectively. Contrary to this, the other device made from white powder did not show a detectable change in base resistance of the sensor. These initial results indicate the potential use of stable TiS_2 nanostructures as a highly selective and sensitive room temperature ammonia sensor.

Keywords 2-D material · TiS_2 nanostructures · Room temperature NH_3 gas sensor · Tmdcs · Liquid exfoliation · Sensitivity

1 Introduction

In past few years transition metal dichalcogenides (TMDCs) have received significant attention due to their intriguing physical properties. This includes, the presence of intrinsic band gap, relatively larger electronic mobility, thermoelectric figure of merit and spin–orbit coupling strength. These features make them attractive for various electronic, spintronic, and thermoelectric applications [1, 2]. TMDCs have general formula MX_2, where M is transition metal (Mo, W or Ti) and X is a chalcogen atom (S, Se or Te). Out of these TMDCs, MoS_2, $MoSe_2$ and WS_2 have been studied extensively and studies on TiS_2 are very rare. Titanium disulfide forms a layered structure in which neighboring layers are stacked via relatively weak van der Waals interactions. Each layer contains titanium atoms that are located in same plane, while sulfur atoms are located on top and below the titanium planes. Therefore, a side view of one TiS_2 layer consists of three planes containing S, Ti and S, respectively. As a result, each titanium atom co-ordinates with six neighbouring sulfur atoms and forms an octahedral geometry where each sulfur atom is connected with three neighbouring titanium atoms. Due to their technological importance as lubricants in petroleum industry, a catalyst, and use in high energy density batteries, they have been studied extensively in bulk form in last three decades [3–6]. But recent advances in vacuum technology and electronic industry have provided impetus to explore the use of these 2-dimensional materials as next generation material for electronics or optoelectronics and thermoelectric devices [7, 8]. This has renewed both experimental as well as theoretical interests in 2-dimensional TMDCs. Their applications are not only limited to these three areas but large surface area-to-volume ratio also signifies their

✉ Sandeep Sharma, sandeepscl@gmail.com | [1]Department of Physics, Guru Nanak Dev University, Amritsar, Punjab 143005, India.

SN Applied Sciences (2020) 2:887 | https://doi.org/10.1007/s42452-020-2647-x

potential use as various sensing devices. Despite technological relevance and increasing interests in TiS_2, very little is known about its usage in sensing application. On the other hand other TMDCs, for instance MoS_2, $MoSe_2$ and WS_2 have been explored extensively for their applications in sensing various gases [9–20]. A fundamental understanding of the interaction between various adsorbed gas molecules and MoS_2 or WS_2 has been developed recently [12, 21, 22]. The sensing mechanism has been understood as conductance modulation of the base channel arising from charge transfer between adsorbed gas molecule and channel [12, 21, 23]. Exposure to basal plane and/or particle size reduction in the nanometer range combined with functionalization with other nanomaterial has emerged as key strategies to improve the sensing capabilities of these materials. This has renewed interests in various other nanostructured forms, for instance nanotubes, nanospheres, nano discs etc. The primarily interests stem from the fact that in nanostructured form they have very large surface area and sometimes a large number of exposed active sites [13], thus proving beneficial for sensing based applications. This has resulted in the development of various exfoliation strategies for the bulk layered material [24]. Mechanical exfoliation offer high quality sheets but cannot be scaled for larger production level [25, 26]. Other possible strategies like liquid-phase exfoliation and or mixed solvent approach, offer high exfoliation yields, better control over size of nanostructures [24]. However, water based exfoliation strategy if applied to TiS_2 presents a significant challenge related to conversion of TiS_2 into TiO_2 via hydrolysis [27–30]. Further, it is expected that with reduced dimensions of the nanostructures, the surface area available for hydrolysis increases and faster transformation is expected. This is indeed the case we have observed and reported below. In present work we investigate the process of liquid-phase exfoliation of TiS_2 in different media, namely de-ionized water (DI–water), DI–water–ethanol mixture, *N*-methyle pyrolidone (NMP), di-methyle formamide (DMF).We will discuss the stability of theses nanostructures using various characterization techniques. Further, these nanostructures were used for making two terminal sensing devices and yielded entirely different results depending upon whether they were processed in water or DMF or NMP. The sensor was exposed to six different analytes (methanol, ethanol, formaldehyde, chloroform, acetone and NH_3) and their response, recovery characteristics were monitored. We conclude our results with the fact that stable TiS_2 nanostructures display strong interaction with ammonia at room temperature whereas those transformed into a white powder do not display such behavior. Therefore, such stable TiS_2 nanostructures can be used as selective and sensitive probe for sensing ammonia even at room temperature. Present results also justify the potential use of scaled nanostructures in sensor devices.

2 Experimental

2.1 Nanostructures and sensor fabrication

Crystalline TiS_2 powder (Sigma-Aldrich, India) was used as received. A probe sonicator (PCI-Analytics, India) was used to exfoliate the crystalline powder. In total five samples S1, S2, S3, S4 and S5 were prepared in different liquid media. At first a mixture of 2 g TiS_2 in 50 ml of de-ionized water was used to prepare two different suspensions of TiS_2 nanostructures. Initially, the above mixture was stirred and probe sonicated for 45 min. Thereafter, a small amount of suspension was removed from this mixture. Suspension was transferred drop-wise on a pre-cleaned glass slide and thereafter it was dried in an oven under ambient conditions at 80 °C. This sample was used for X rays diffraction (XRD) and Raman spectroscopy measurements and named as S1. For scanning electron microscopy measurements SEM) the suspension was directly transferred on carbon tape and dried. Similarly, for high resolution transmission electron microscopy (HR-TEM) measurements, a diluted drop of same suspension was poured on a carbon coated grid and dried.

The starting mixture was again probe-sonicated for another 15 min and samples for XRD, Raman, SEM and HR-TEM were prepared as described above. The newly prepared sample on glass slide was named S2. Note that same suspensions obtained after 45 and 60 min of sonication were also used for optical measurements. They were also named S1 and S2 respectively. In addition to these two samples, three more samples (S3, S4 and S5) were prepared in di-methyle formamide (DMF), *N*-methyle pyrolidone NMP) and DI water–ethanol mixture, respectively. These three samples were processed for 30 min and corresponding suspension was used only for optical characterization. A brief description of samples is given in Table 1. Further, to make gas sensing measurements, two terminal devices were made on a glass substrate with pre-deposited electrical contacts. Contact electrodes were deposited on glass substrate via thermal evaporation of aluminium. The powder obtained after sonications were dried in a vacuum oven for nearly half an hour and thereafter mixed with small amount of DI–water to make a paste. This paste was applied on glass substrates with pre-deposited electrical contacts and this way four (TiS_2 powder obtained after processing in DMF, NMP, Water–etahnol mixture and water) different two-terminal devices were made. Note that in latter two cases the obtained powder was white in colour. Sensing measurements were performed using a

Table 1 Description of various samples prepared in different media

Sample name	Media	Processing time (mnt)
S1	DI–water	45
S2	DI–water	60
A	–	For TEM
B	–	For TEM
S3	DMF	30
S4	NMP	30
S5	DI + ethanol	30

Note that sample A was prepared from S2 immediately after sonication and B was prepared from same powder (S2) that turned into a white powder after a few days

home built apparatus consisting a 40 L chamber, temperature controlled oven, circulating fan, and a simple potentiometer. In this chamber various concentrations of gas molecules could be obtained by vaporizing the corresponding liquid compound. The ammonia concentration (in ppm) can be calculated from known molecular weight (17.031 g/mole) and its density (0.67 g/ml) as follows: The volume of ammonia at NTP (Normal Temperature and pressure) equals (molecular weight/density) 25.42 ml. Therefore at NTP 25.42 ml of ammonia will contain 6.023×10^{23} molecules of ammonia. From here one can calculate the number of molecule for a known volume of ammonia injected into the measurement chamber. The gas concentration in ppm is evaluated using the known number (6.023×10^{23}) of air gas molecule in a volume of 22.4 L at NTP and number of ammonia molecules in known volume of ammonia injected into the measurement chamber.

2.2 Material characterization

XRD diffractograms were acquired using D8 Bruker with Cu Kα line. High-resolution transmission electron micrographs were acquired using JEOL JEM-2100 operating at 200 keV. The selected area electron diffraction (SAED) pattern was acquired from the same samples. The Raman spectra of these samples were taken with Renishaw Invia Reflex micro Raman spectrometer using visible excitation (488 nm). Optical absorption properties were measured with Shimadzu UV-2450 spectrophotometer. Photoluminescence emission from nanostructures was recorded by using Perkin Elmer LS55 fluorescence spectrometer.

3 Results and discussion

Figure 1 shows the images of TiS_2 nanosheets in different liquid media as produced, after 1 and 3 months. It is clear that suspension obtained in DMF is more stable and no

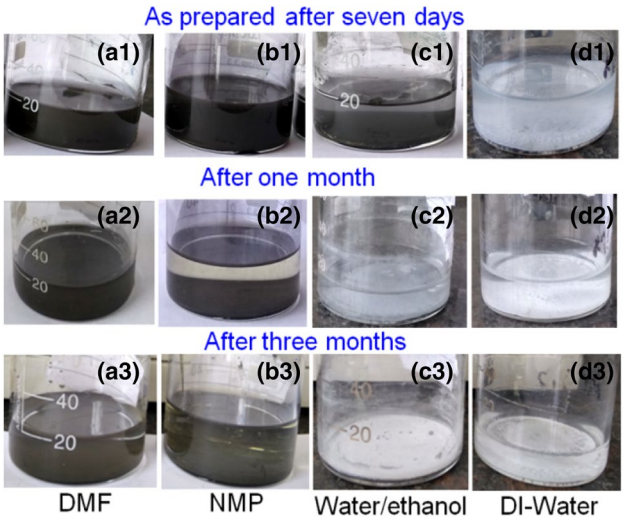

Fig. 1 TiS_2 nanostructures prepared in different liquid media. Images displaying unstable nature of the nanostructures with passage of time. For more details refer to the text

colour change is observed even after a few months. On the other hand, a uniform Suspension is obtained in NMP; this is followed by agglomeration and precipitation of the nanosheets with the passage of time. Entirely different picture can be seen with the TiS_2 suspension obtained in DI–water, and DI–water/ethanol mixture. In these two cases the initial black coloured suspension of TiS_2 first undergoes agglomeration followed by precipitation and with the passage of time the precipitate colour slowly changes to white. These changes are slower in water–ethanol mixture as compared to pure DI–water. In order to probe these changes systematically we have performed optical and vibrational measurements on the obtained TiS_2 nanostructures. In order to use these TiS_2 nanostructures for various applications, it is crucial to understand this transformation so that stable suspensions can be obtained and further used. Historically, the colour change on TiS_2 nanosheets has been attributed to the oxidation. In presence of water molecules, TiS_2 spontaneously change to TiO_2 via the formation of intermediate species TiSO and releasing H_2S gas as a by product [27–30].

Figure 2 displays the X-ray diffractogram of bulk crystalline powder, S1 and S2. The diffraction pattern for bulk sample matches well with hexagonal TiS_2 (JCPDS-74 1141; space group p3m1, a = 3.39 Å, c = 5.69 Å). The XRD from a bulk crystalline TiS_2 powder displays a sharp intense peak corresponding to (001) planes, implying preferred c-axis orientation [31, 32]. Further, we note that after exfoliation, relative intensity of most of the planes as compared with (001) plane has reduced and hence the exfoliated thin sheets of TiS_2 exhibit c-axis orientation. This implies successful exfoliation of the starting bulk material. We also

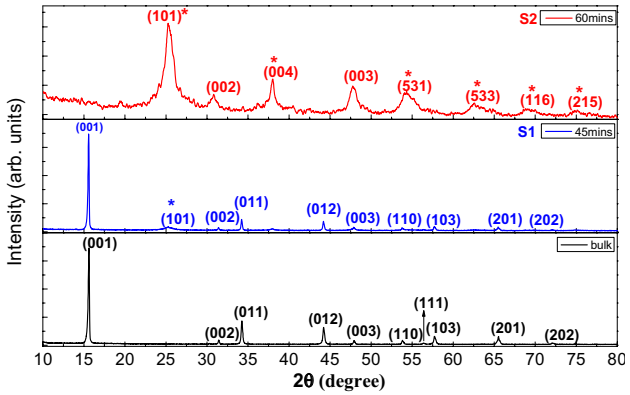

Fig. 2 The XRD patterns of bulk, S1 and S2 TiS_2 samples. Note that S1 and S2 are processed in DI water for 45 and 60 min, respectively

observed that in sample S1 a new peak at 25.33° marked with '*' has appeared. After analysis it is attributed to (101) planes from Anatase TiO_2 (JCPDS-84-1286; space group I41/amd, a = 3.78 Å, c = 9.50 Å). In sample S2, the peak intensity corresponding to (101) planes has increased and other peaks (004), (531), (533), (116) and (215) belonging to anatase TiO_2 have appeared. As shown in Fig. 2, the (001) and (011) peaks corresponding to TiS_2 slowly disappeared and new peaks belonging to titanium oxide have appeared. We also note that peak width broadens with increase in the processing time. This implies a significant reduction in crystallite size.

The morphology and crystal structure of TiS_2 nanostructures were investigated using scanning electron microscopy and high resolution transmission electron microscopy. The SEM image from the TiS_2 is shown in Fig. 3. Image (a) displays the layered crystallites with size ranging from sub-micrometer to a few micrometers. Image (b) also displays similar information at higher magnification. For TEM imaging two samples were made. One of the samples was made immediately from TiS_2 nanostructures processed in DI–water and named as sample A. The second sample was made from the powder that turned into white colour (TiO_2) and was named as sample B. Figure 4a–c shows HR-TEM image of the sample A. The images confirmed the crystalline character of the thin TiS_2 nano sheets. The digitally filtered images in the insets confirmed the presence of (001), (002) and (220) planes with inter-planer spacing of 5.7 Å, 2.8 Å and 3.5 Å, respectively. During liquid exfoliation these sheets may bundeled up. This is clear from left inset in Fig. 4a. Further, lower right inset in the same figure represents the formation of edge dislocations. Thus, probe sonication has not only reduced the dimensions of the starting bulk crystalline powder but also resulted in the formation of defects which may influence optical and electronic properties of the material. The Selected area electron diffraction (SAED) pattern in Fig. 4d further confirms the presence of various planes earlier noted from XRD pattern and HR-TEM images from the same sample. The SAED pattern displays various concentric rings, a signature of polycrystalline nature of sample. However, it should be noted that after probe sonication the suspension containing various thin nano sheets of layered material become unstable and latter may restack them at different angles w.r.t. original crystal orientation. In that case stacked layers (at different angles) may give rise to such ring pattern. The SAED image contains reflections associated with c-axis, namely (001), (002) and relatively faint (003), indicating the presence of thicker sheets of TiS_2. In case of bulk TiS_2 the c-axis is perpendicular to the planes that are associated with S–Ti–S trilayers. Thus electron diffraction pattern is consistent with the XRD pattern and indicates that nanostructures are a few layers thick. Further, similar measurements on sample B are shown in Fig. 4e, f. The inset in (e) highlights the area from where diffraction pattern has been taken. The SAED pattern displays blurred and wide rings corresponding to (004) and (215) planes of TiO_2.

Raman spectroscopy is a powerful non-destructive technique that simultaneously provides structural and electronic information. One can identify unwanted

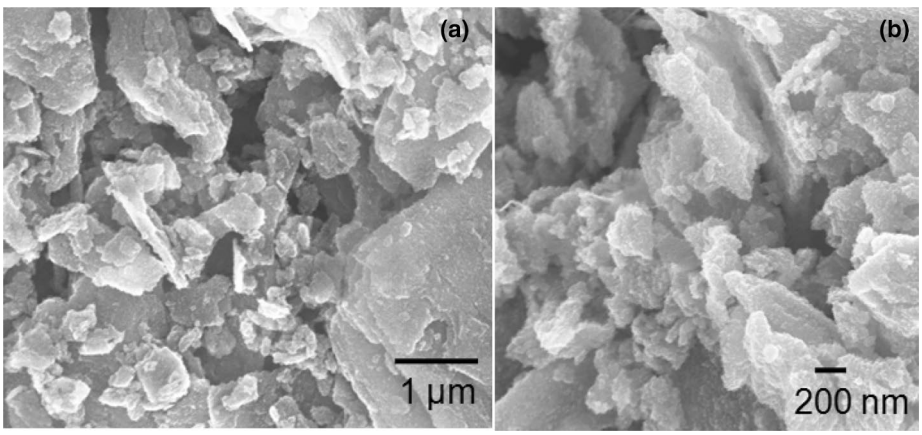

Fig. 3 **a** Low magnification and **b** high magnification scanning electron microscopy images of TiS_2

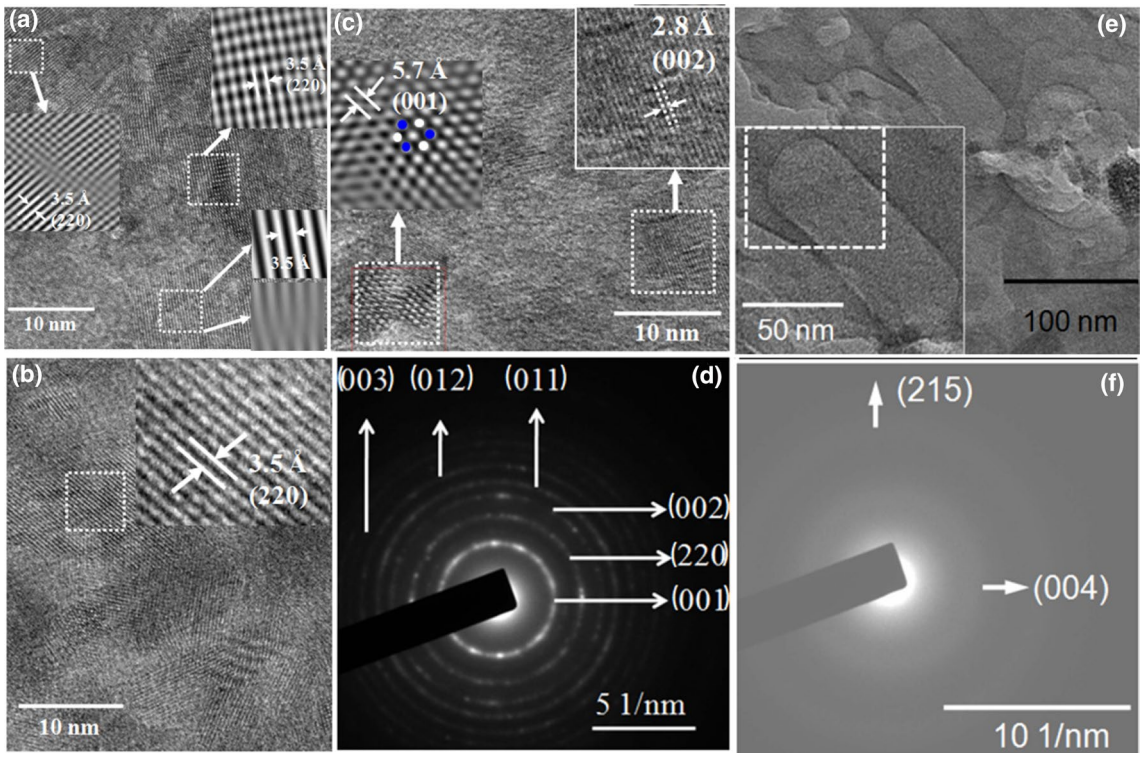

Fig. 4 TEM images **a**, **b** for sample S1, **c**, **d** for S2, both freshly prepared in DI–water. Images **e**, **f** correspond to same sample that turned into white powder (TiO_2)

by-products or even phase change or chemical modifications that are introduced during the preparation. In order to facilitate a comparison between processed samples and bulk crystalline TiS_2 powder we recall that lattice vibrations of TiS_2 under irreducible representation of the zone-center phonon Modes are expressed as:

$$\Gamma = A_{1g}(R) + E_g(R) + 2E_u(IR) + 2A_{2u}(IR)$$

where R and IR denote, respectively, Raman and infrared active modes. The corresponding atomic displacements for these modes at Γ point are shown in Fig. 5. The Ti atom which is located at the inversion center is static in Raman modes whereas it is active in the IR modes. In E_g mode, the adjacent S sheets moves within their plane in anti-phase with each other while in A_{1g} mode they oscillate out-of-plane in anti-phase manner. The E_u mode consists of in-plane sheets gliding motions where S and Ti atoms move out-of-phase. The A_{2u} mode on the other hand consists of out-of-plane vibrations of Ti and S atoms, with Ti and S atoms moving out-of-phase with each other. Table 2 gives the peak position corresponding to various Raman active modes in TiS_2. There is a little spread in the values reported by various researchers. We have performed Raman spectroscopy of both crystalline TiS_2 powder and their nanostructures. The data acquired using 488 nm excitation is

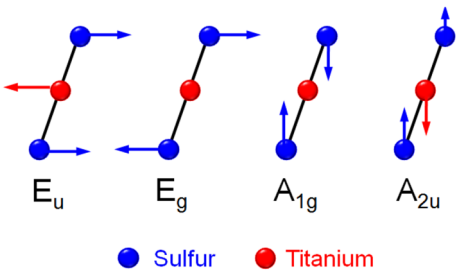

Fig. 5 Schematic illustration of various Raman active modes in TiS_2. Arrows indicate the vibration of Ti or S atoms in particular mode

shown in Fig. 6a, b. Peak positions corresponding to various vibrational modes are summarized in Table 3. As we see, in Fig. 6a, the Raman spectroscopy revealed three primary peaks at 226.89 cm^{-1} (assigned to E_g), 327.51 cm^{-1} (assigned to A_{1g}) and 379.5 cm^{-1} corresponding to A_{2u}. These three modes correspond to TiS_2 [33–35]. In addition to these three modes, the data also revealed two modes with relatively lower intensity at 151.7 cm^{-1} and at 631.7 cm^{-1} (assigned as E_g) due to anatase TiO_2. Let us take a look at Raman spectra from samples S1 and S2. The data in Table 3 indicates that mode A_{1g} stiffens as we move from bulk to scaled nanostructures. This is contrary to what has been noticed for scaled TiS_2 sheet [27] with only one, two,

Table 2 Various phonon modes positions in TiS_2

Mode name	Mode position (cm^{-1})
E_u(IR)	180
	175
E_g(R)	233
	234
	226
A_{1g}(R)	328
	335
	332
	330
A_{2u}(IR)	372
	379

Here R stands for Raman mode and IR is infrared active modes

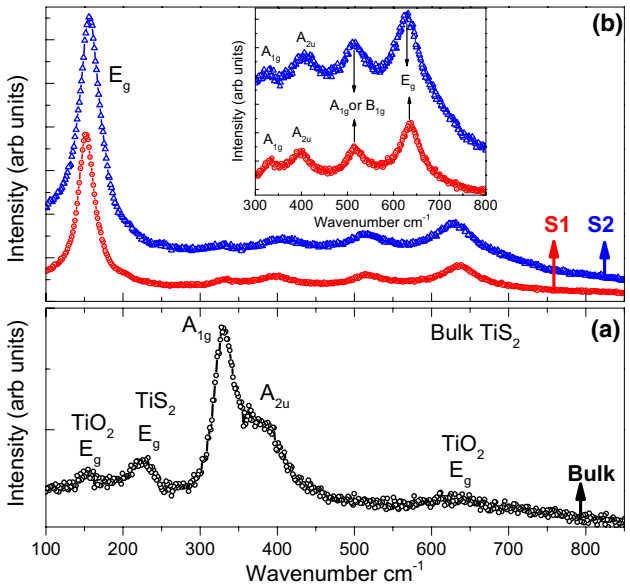

Fig. 6 Room temperature Raman spectra of different samples with $\lambda_{exc} = 488$ nm

four and five layers. These results also differ from Raman spectra obtained from scaled nanostructures of WS_2 and MoS_2 where A_{1g} and $E^1{}_{2g}$ modes soften [36, 37]. Therefore, the observed shift in A1g mode might arise from scaled nanostructures. There is lack of theoretical calculation for such scaled nanostructures. Further, we see, the Raman spectra are dominated by intense peak E_g at ≈ 151 cm^{-1}. The modes arising due to TiS_2 have relatively lower intensity as compared with those coming from TiO_2. Further, the intensity of modes A_{1g} (at 514.54 cm^{-1}, 513.2 cm^{-1}) and E_g (at 638.3 cm^{-1}, 632.0 cm^{-1}) has increased from sample S1 to S2. A better idea can be gauged from the intensity ratio between A_{1g} mode (from TiS_2) and E_g mode (close

Table 3 Peak positions for various Raman active modes of TiS_2 nanostructures and TiO_2 phase at an excitation wavelength of 488 nm

Type	Mode (cm^{-1})	Sample		
		Bulk	S1	S2
TiS_2	E_u(IR)	–	–	–
–	E_g	226.89	–	–
–	A_{1g}	327.51	332.98	328.87
–	A_{2u}(IR)	379.5	395.4	402.5
TiO_2				
–	B_{1g}	–	395.4	402.5
–	E_g	151.7	150.31	155.91
–	A_{1g} or B_{1g}	–	514.54	513.2
–	Eg	631.7	638.3	632.0
Intensity ratio	A_{1g}/E_g	2.9	0.34	0.08

The last row gives the intensity ratios for the A_{1g} mode (from TiS_2) and E_g mode from TiO_2

to 150 cm^{-1}) from TiO_2. This ratio is given in last row of Table 3. It is clear that intensity ratio changes from 2.9 to 0.34 to 0.08 in bulk sample, S1 and S2, respectively. Reductions in intensity ratio of these two modes suggest that with the passage of time TiS_2 changes to TiO_2 giving rise to intense peaks belonging to latter. This transformation is faster in sample which is probe sonicated for larger duration of time. Thus, suggesting that nanostructures with larger available surface area (smaller size) quickly change into TiO_2.

UV–Vis spectroscopy (Shimadzu) was used to investigate optical absorption of obtained TiS_2 nanostructures. The results for two samples S1 and S2 prepared in deionized water are displayed in Figs. 7 and 8. After obtaining the nanostructures, the absorption spectrum was measured. Thereafter, the measurements were repeated two times after a gap of 3 months. As we see, the onset of absorption appears even at 600 nm and it increase towards lower wavelengths. A small absorption hump can be seen between 300 and 400 nm. Clearly, as TiS_2 changes into TiO_2, this absorption peak between 300 and 400 nm grows with time for both samples. This is further corroborated by PL studies (Fig. 10), Showing a new emission peak centred around 400 nm (with 250 nm excitation). It is known that nanometre sized TiO_2 exhibits emission in this range. Thus, we conclude that these features originate from titanium dioxide [38]. The absorption spectrum for three more freshly prepared samples in NMP, DMF and DI water/ethanol mixture is also shown in Fig. 9. We notice a broad absorption between 450 and 800 nm in all samples. Though, these absorption features are less pronounced in samples obtained in DMF and water–ethanol mixture. This broad absorption corresponds to bulk TiS_2 [39]. Therefore,

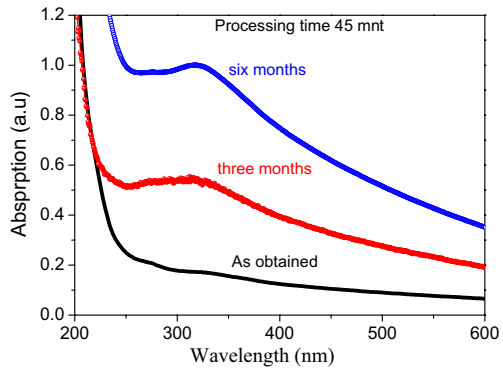

Fig. 7 Change in optical absorption with the passage of time. Data shown for TiS_2 nanostructures processed in de-ionized water for 45 min

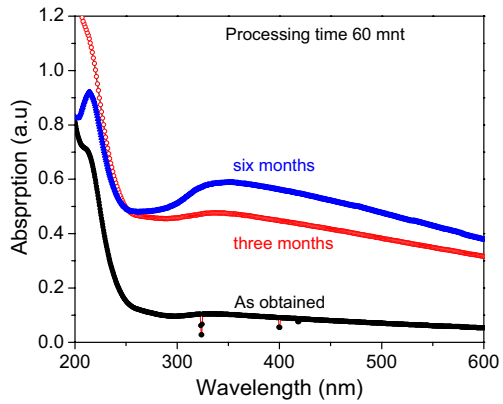

Fig. 8 Change in optical absorption with the passage of time. Data shown for TiS2 nanostructures processed in deionized water for 60 min

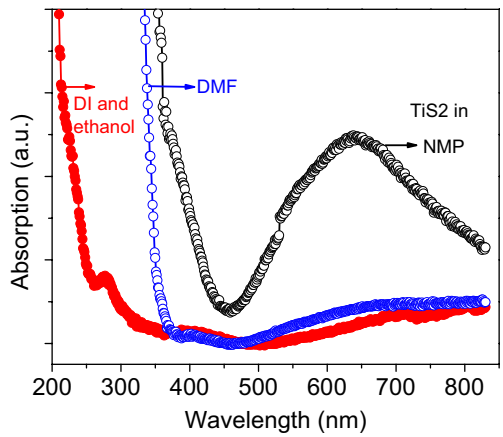

Fig. 9 Optical absorption spectrum for TiS_2 nanostructures prepared in NMP, DMF and DI water ethanol mixture

NMP is least effective in obtaining TiS_2 nanostructures. Contrary to this, the absorption spectrum of sample S5 contains an absorption features at lower wavelength and a peak around 270 nm. Such differences in absorption pattern from same starting material might arise due to different liquid media chosen for probe sonication. Recently, similar features have been noticed with other TMDCs, for instance WS_2 [40]. In short, the parameters such as surface tension and relative permittivity etc. play a major role to judge the effectiveness of a solvent used as dispersive media [41]. Previous studies have shown that TiS_2 processed in water displays immediate aggregation followed by oxidation into TiO_2 [27]. The feature around 270 nm was assigned to immediate conversion of TiS_2 into TiO_2 within a period of five days. Indeed this is in line with the visual inspection of the samples prepared in our study. Therefore, presence of water molecules has immediate consequences in transforming TiS_2 into TiO_2 and changing former colour from black to white. In order to further explore the properties of the nanostructures, emission spectra were acquired on different samples and data is shown in Figs. 10 and 11. Figure 10 displays the emission spectra for samples S1 and S2 at two different excitations. As we see, the emission spectra display different features for same excitation with the passage of time. Similar features can be seen in sample S5 also. A more relevant detail can be seen from the deconvoluted emission spectra from samples S1, S2, S3 and S4 as shown in Fig. 12. As we see, in sample S1 and S2 the emission features evolve with time. Note that these two samples turn into white powder with the passage of time and this has been attributed to transformation of TiS_2 into TiO_2. In literature the emission peaks in Fig. 14b has been well documented and attributed to various defects level in TiO_2 [45]. On the other hand, the emission spectra in (c) and (d) does not display any such change and various emission peaks reflects the intrinsic feature from TiS_2. A wide emission spectra might arise due to poly-dispersity of the obtained nanostructures and/or presence of defects in obtained scaled nanostructures [40]. Therefore, the data indicates that suspension obtained in DMF and NMP are stable as compared with others.

The TiS_2 nanostructures possess a very large surface-to volume ratio and hence can be used for gas sensing applications. For this purpose we prepared four different two-terminal devices from powder obtained after probe sonication of TiS_2 in DMF, NMP, water–ethanol mixture and DI–water alone. Note that in latter two cases the powder that has turned completely into white colour was used. The separation between electrodes was kept at 5 mm. A representative resistance vs. time measurement on one of devices prepared from TiS_2 nanostructures obtained in DMF is shown in Fig. 13. Initially, the resistance of the device was measured in air and later ammonia was inserted into the chamber. As we see, the

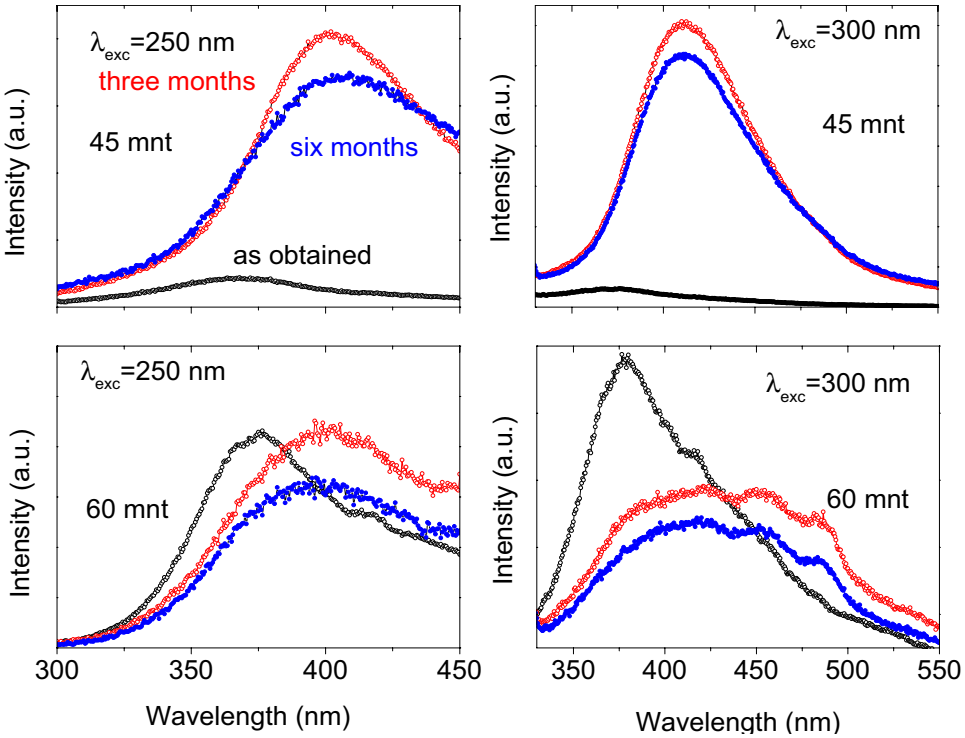

Fig. 10 PL spectra of TiS_2 nanostructures processed in de-ionized water for 45 and 60 min. The spectra were obtained on same sample after a gap of 3 months

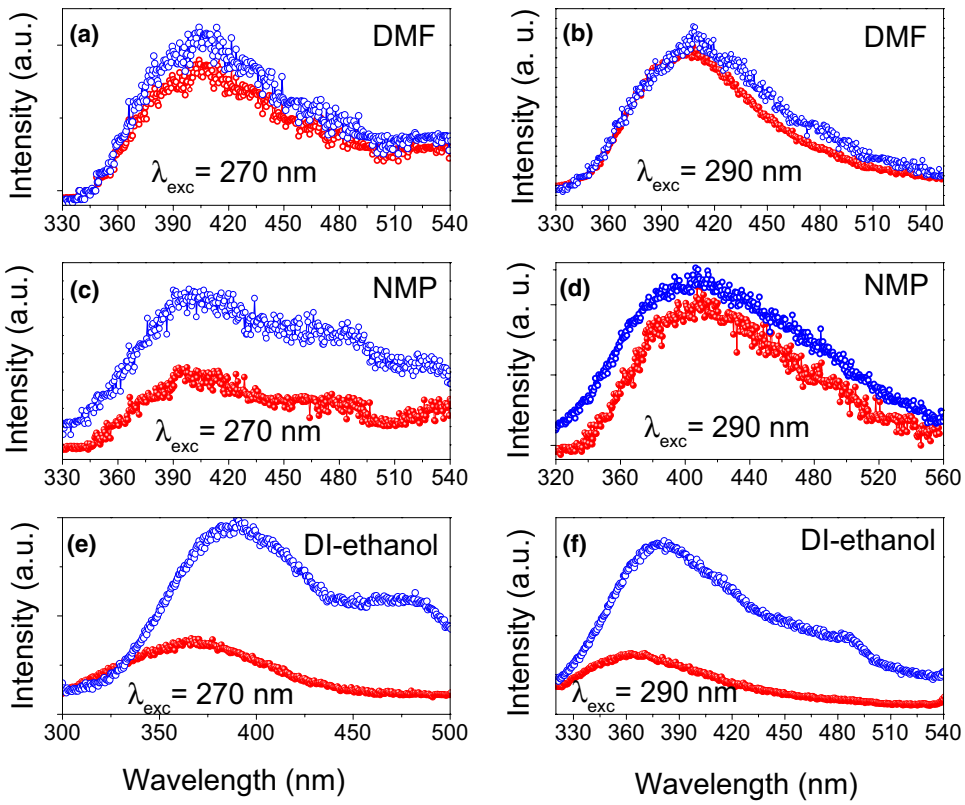

Fig. 11 PL spectra of TiS_2 nanostructures processed in different media. Two spectra in each figure correspond to same sample but measured after a gap of 1 month. Lower spectra measured right after processing and upper one measured after a gap of 1 month

device resistance in air is close to 13.5 M Ω. When ammonia is inserted into the chamber, the resistance reduces to a value of approximately 3 M Ω. After removing the ammonia gas, the resistance of sensing device slowly recovers to its original value in air. This, together with the fact that ammonia molecules behave like electron donor, establish n-type behaviour

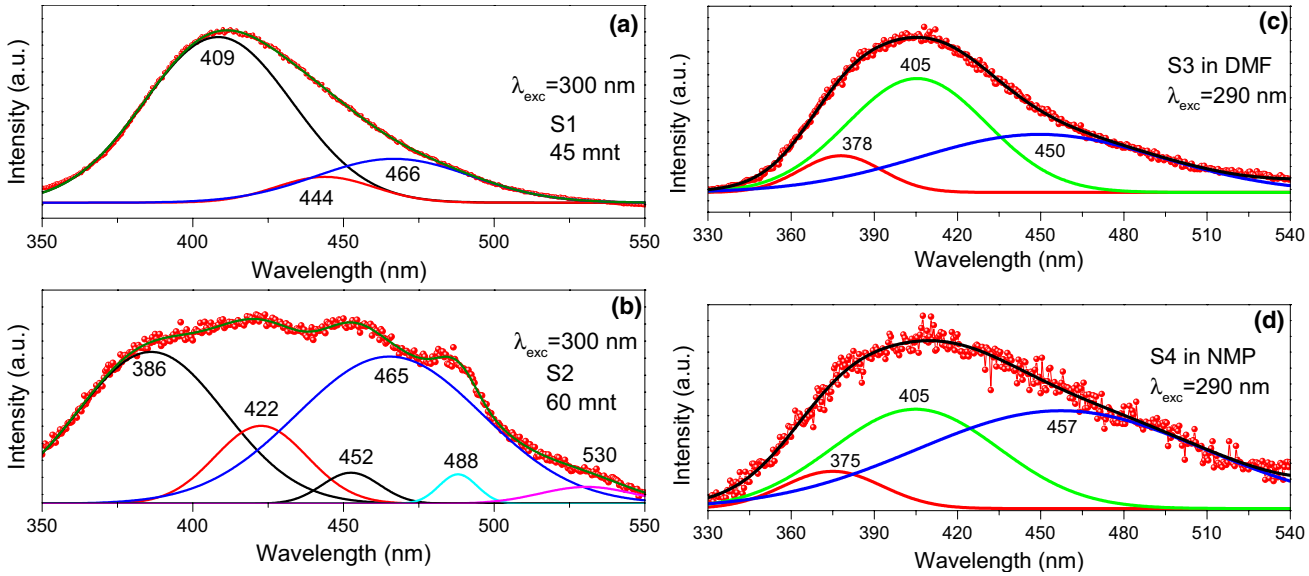

Fig. 12 **a**, **b** De-convoluted emission spectra (obtained after 3 months) from samples S1, S2 (**c**, **d**) S3 and S4. Data displaying the differences between emission features from same starting material (TiS_2)

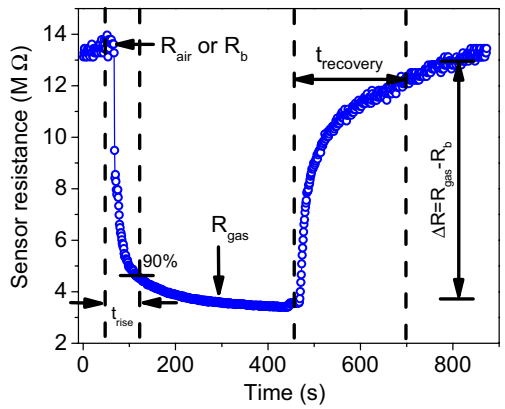

Fig. 13 Two-terminal sensor response to ammonia at room temperature and definition response (t_{rise}) and recovery ($t_{recovery}$) time

of the device. This Figure also defines the rise time (t_{rise}) as the time taken by the sensor to achieve ninety percent of the maximum change in the resistance value. Similarly, the recovery time ($t_{recovery}$) is defined as the time taken by the sensor to change its value from maximum resistance value to ten percent above the minimum value. This Figure also defines the maximum change in resistance as $\Delta R = |R_{gas} - R_b|$, where R_{gas} is minimum resistance in presence of gas and R_b is the resistance measured in air. From here the relative response is defined as $\Delta R/R_b$. Similar measurements were repeated on other three devices and data is shown in Fig. 14. In Fig. 14a a comparison between four different devices is shown when they were exposed to 200 ppm of ammonia at 30 °C and relative humidity level of 40%. A clear signal was obtained from devices made from TiS_2 processed in DMF and NMP whereas other two devices displayed poor signal to noise ratio. For this reason rest of the measurements were performed only on first device made from TiS_2 processed in DMF. Figure 14b displays the response-recovery transient for the device at different ammonia concentrations. In (c) absolute relative-response $\Delta R/R_b$ (in percent) is shown. As we see, a nearly linear increase with ammonia concentration is observed. The long term durability is another figure of merit of a sensor device. In (d), a stable behaviour of the device is visible when exposed to three continuous cycles of ammonia (200 ppm). The relative response was within 72 ± 2% and the rise time and recovery time are respectively, 72 ± 7 s and 165 ± 10 s. Further, the cross sensitivity of sensor device was checked for five other gas molecules (ethanol, formaldehyde, methanol, chloroform and benzene) and results are shown in Fig. 15. A clear signal for ammonia compared with other gas molecules indicates highly selective behaviour of TiS_2 based sensor. In case of ethanol, a relative response of 12 ± 3% is obtained. A relatively very poor signal has been obtained for other analytes. This indicates highly selective nature of TiS_2 nanostructures towards ammonia.

4 Conclusions

The TiS_2 nanostructures were prepared in different liquid media. The initial visual inspection revealed clear transformation of black TiS_2 into a white TiO_2 powder. This conversion process was faster for TiS_2 processed in pure water as compared to the one processed in DI–water–ethanol

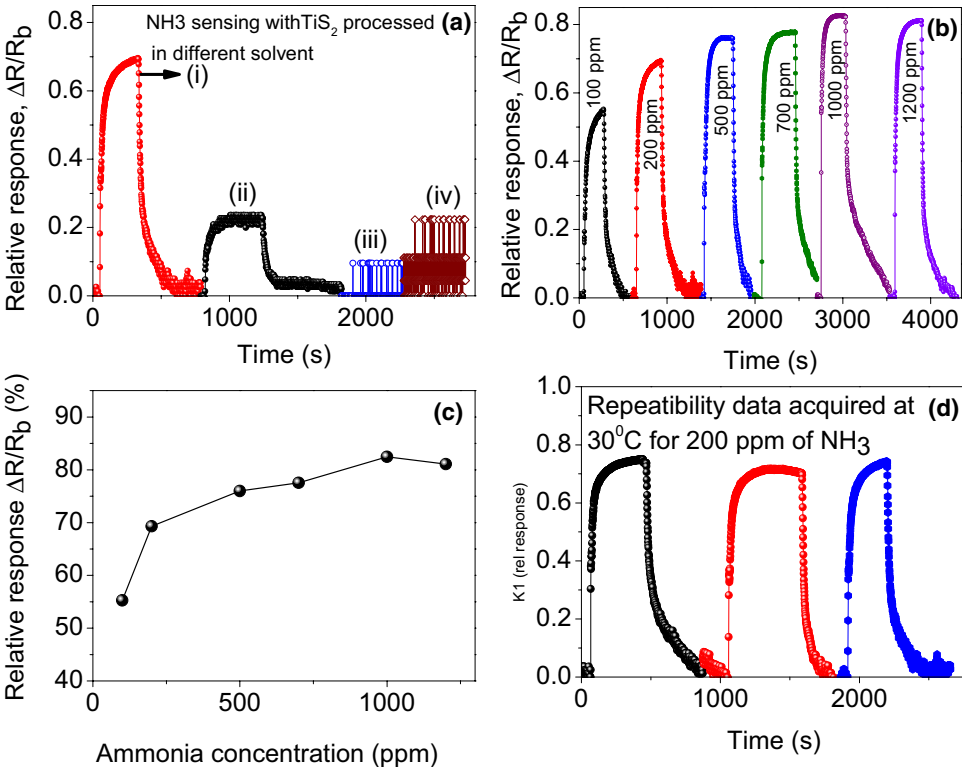

Fig. 14 **a** Relative response from sensor devices made from TiS_2 processed in (i) DMF (ii) NMP, (iii) Ethanol–Water, (E–W) and (iv) Water (W). **b**, **c** Relative-response of TiS2 sensor for different ammonia concentrations. **d** Repeatability of sensor devices at room temperature for 200 ppm of ammonia concentration

mixture. This transformation was further established using various structural, optical and vibrational measurements. The XRD data showed the presence of various peaks namely (101), (004) and (215) corresponding to anatase TiO_2. These peaks appear in XRD diffractogram of the processed TiS_2 sample with the passage of time. The SAED pattern from freshly prepared TiS_2 samples displayed concentric rings belonging to various planes of TiS_2. Similar analysis on sample that turned into white powder revealed wide and blurred rings corresponding to (004) and (215) planes of TiO_2. Further, Raman spectroscopy

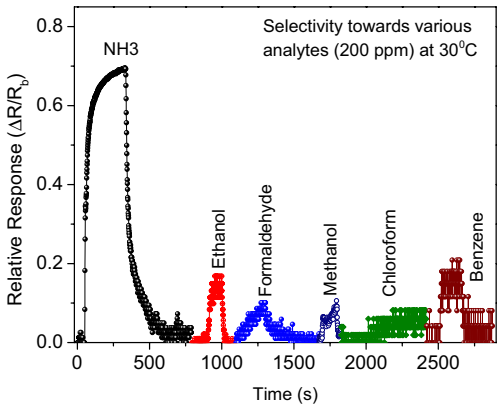

Fig. 15 Selectivity behaviour of TiS_2 sensor towards various gaseous molecules

measurements on bulk TiS_2 have shown the presence of various Raman active modes corresponding to vibrations of Ti and S atoms. The minute traces of TiO_2 were noticeable from the presence of two E_g modes at 151.7 cm^{-1} and 631.7 cm^{-1}. These two modes correspond to TiO_2. The intensity of E_g mode at 151.7 cm^{-1} increases with the passage of time. Further, the intensity ratio between the A_{1g} mode (from TiS_2) and E_g mode (from TiO_2) reduced from 2.9 (bulk) to 0.34 (S1) to 0.08 (S2). This reduction in intensity indicates the conversion of TiS_2 into TiO_2. These observations were further corroborated by the optical measurements on the obtained TiS_2 suspensions. The optical absorption was enhanced in certain spectral region. This enhanced absorption corresponds to absorption from TiO_2. Further, PL-emission spectra also revealed that TiS_2 nanostructures are more stable in DMF and NMP as compared with water or water ethanol mixture. In latter two cases in presence of water molecules the TiS_2 undergoes oxidation to form TiO_2. The black and white coloured nanostructures when used for making two terminal sensor devices, displayed entirely different behaviour. The former showed n-type character with nearly 72% response to 200 ppm of ammonia at room temperature whereas no detectable change was observed in the latter case, similar to previous results on TiO_2 based sensor where TiO_2 was obtained via wet oxidation [42]. The gas sensing measurements in presence of other analytes such as ethanol, methanol, formaldehyde, acetone etc. didn't yield

any change in the base resistance. This behaviour clearly distinguishes the highly sensitive and selective nature of stable TiS_2 nanostructures from white TiO_2 powder. At the end, we have successfully prepared stable TiS_2 nanostructures in DMF and NMP. These nanostructures were successfully employed for making two terminal sensor devices. The decrease in resistance after exposure to ammonia molecules clearly reveals their n-type behaviour. The obtained rise time and recovery time are respectively, 72 ± 7 s and 165 ± 10 s. Unlike MoS_2 and WS_2, the fundamental understanding of interaction between gas molecules and TiS_2 is lacking and further theoretical as well as experimental investigations are required. For instance, recent theoretical investigations have revealed a negative adsorption energy for NH_3 on MoS_2 (− 250 meV) and WS_2 (− 216 meV), implying adsorption process to be stable and exothermic in nature [43, 44]. These first principle calculations also revealed reducing nature of NH_3 molecules, implying charge transfer from adsorbed NH_3 gas molecules to the underlying semiconducting channel, TiS_2 in present case. The experimental work in understanding the selectivity behaviour and interaction mechanism is underway and will be reported in future work. Present work justifies the potential use of the TiS_2 nanostructures as a room temperature gas sensing material.

Acknowledgements This work was supported by DST-New Delhi, India under the Grant No. EMR/2016-007483.

Compliance with ethical standards

Conflict of interest The authors declare no competing financial interest.

References

1. Chen KX, Wang XM, Mo DC, Lyu SS (2015) Thermoelectric properties of transition metal dichalcogenides: From monolayers to nanotubes. J Phys Chem C 119:26706–26711
2. Wang QH, Kalantar ZK, Kis A, Coleman JN, Strano MS (2012) Electronics and optoelectronics of two-dimensional transition metal dichalcogenides. Nat Nano 7:699–712
3. Schwarz J, Contescu C, Putyera K (2004) Encyclopedia of nanoscience and nanotechnology. Marcel Dekker, New York
4. Wilson JA, Salvo FJD, Mahajan S (2001) Charge-density waves and superlattices in the metallic layered transition metal dichalcogenides. Adv Phys 50:1171–1248
5. Friend R, Yoffe A (1987) Electronic properties of intercalation complexes of the transition metal dichalcogenides. Adv Phys 36:1–94
6. Whittingham MS (1976) Electrical energy storage and intercalation chemistry. Science 192:1126–1127
7. Kong S, Wu T, Yuan M, Huang Z, Meng QL, Jiang Q, Zhuang W, Jiang P, Bao X (2017) Dramatically enhanced thermoelectric performance of MoS_2 by introducing MoO_2 nanoinclusions. J Mater Chem A 5:2004–2011
8. Wang QH, Zadeh KK, Kis A, Coleman JN, Strano MS (2012) Electronics and optoelectronics of two-dimensional transition metal dichalcogenides. Nat Nanotechnol 7:699–712
9. Agrawal AV, Kumar R, Venkatesan S, Zakhidov A, Zhu Z, Bao J, Kumar M (2017) Fast detection and low power hydrogen sensor using edge-oriented vertically aligned 3-d network of MoS_2 flakes at room temperature. Appl Phys Lett 111:093102
10. Asres GA, Baldovi JJ, Dombovari A, Jarvinen T et al (2018) Ultrasensitive H_2S gas sensors based on p-type WS_2 hybrid materials. Nano Res 11:4215–4224
11. Baek J, Yin D, Na L, Omkaram I, Jung C, Im H, Hong S, Kim SM, Hong YK, Hur J, Yoon Y, Kim S (2017) Highly sensitive chemical gas detecting transistor based on highly crystalline CVD-grown $MoSe_2$ films. Nano Res 10:1861–1871
12. Cho B, Hahm MG, Choi M, Yoon J et al (2015) Charge transfer-based gas sensing using atomic-layer MoS_2. Sci Rep 5:8052
13. Cho SY, Kim SJ, Lee Y, Kim JS, Jung WB, Yoo HW, Kim J, Jung HT (2015) Highly enhanced gas adsorption properties in vertically aligned MoS_2 layers. ACS Nano 9:9314–9321
14. Choi SY, Kim Y, Chung HS, Kim AR, Kwon JD, Park J, Kim YL, Kwon SH, Hahm MG, Cho B (2017) Effect of Nb doping on chemical sensing performance of two-dimensional layered $MoSe_2$. ACS Appl Mater Interfaces 9:3817–3823
15. Huang KJ, Liu YJ, Wang HB, Gan T, Liu YM, Wang LL (2014) Signal amplification for electrochemical dna biosensor based on two dimensional graphene analogue tungsten sulphide graphene composites and gold nanoparticles. Sens Actuators B 191:828–836
16. Kim YH, Kim KY, Choi YR, Shim YS, Jeon JM, Lee JH, Kim SY, Han S, Jang HW (2016) Ultrasensitive reversible oxygen sensing by using liquid-exfoliated MoS_2 nanoparticles. J Mater Chem A 4:6070–6076
17. Ko KY, Song JG, Kim Y, Choi T, Shin S, Lee CW, Lee K, Koo J, Lee H, Kim J, Lee T, Park J, Kim H (2016) Improvement of gas-sensing performance of large-area tungsten disulfide nanosheets by surface functionalization. ACS Nano 10:9287
18. Late DJ, Doneux T, Bougouma M (2014) Single-layer $MoSe_2$ based NH_3 gas sensor. Appl Phys Lett 105:233103
19. Late DJ, Huang YK, Liu B, Acharya J, Shirodkar SN, Luo J, Yan A, Charles D, Waghmare UV, Dravid VP, Rao CNR (2013) Sensing behavior of atomically thin-layered MoS_2 transistors. ACS Nano 7:4879–4891
20. Lee K, Gatensby R, McEvoy N, Hallam T, Duesberg GS (2013) High performance sensors based on molybdenum disulfide thin films. Adv Mater 25:6699–6702
21. Zhou C, Yang W, Zhu H (2015) Mechanism of charge transfer and its impact on fermi-level pinning for gas molecules adsorbed on monolayer WS_2. J Chem Phys 142:214704
22. Zhou CJ, Yang WH, Wu YP, Lin W, Zhu HL (2015) Theoretical study of the interaction of electron donor and acceptor molecules with monolayer WS_2. J Phys D Appl Phys 48:285303
23. Li BL, Wang J, Zou HL, Garaj S, Lim CT, Xie J, Li NB, Leong DT (2016) Low-dimensional transition metal dichalcogenide nanostructures based sensors. Adv Func Mater 26:7034–7056
24. Brent J, Savjani NBP (2017) Synthetic approaches to two dimensional transition metal dichalcogenide nano sheets. Prog Mater Sci 89:411–478
25. Golberg D (2011) Exfoliating the inorganics Nature. Nanotechnology 6:200–201
26. Frindt RF (1966) Single crystals of MoS_2 several molecular layers thick. J Appl Phys 37:1928–1929
27. Sherrell PC, Sharda K, Grotta C, Ranalli J, Sokolikova MS, Pesci FM, Palczynski P, Bemmer VL, Mattevi C (2018) Thickness-dependent characterization of chemically exfoliated TiS_2 nanosheets. ACS Omega 3:8655–8662

28. Park KH, Choi J, Kim HJ, Oh DH, Ahn JR, Son S (2008) Unstable single-layered colloidal TiS_2 nanodisks. Small 4(7):945–950
29. Cucinotta CS, Dolui K, Pettersson H, Ramasse QM, Long E, O'Brain SE, Nicolosi V, Sanvito S (2015) Electronic properties and chemical reactivity of TiS_2 nano flakes. J Phys Chem C 119:15707–15715
30. Martinez H, Auriel C, Gonbeau D, Loudet M, Guillouzo G, Pfister-Guillouzo G (1996) Studies of 1T TiS_2 by STM, AFM and XPS: the mechanism of hydrolysis in air. Appl Surf Sci 93:231–235
31. Lin C, Zhu X, Feng J, Wu C, Hu S, Peng J, Guo Y, Peng L, Zhao J, Huang J, Yang J, Xie Y (2013) Hydrogen-incorporated TiS_2 ultrathin nanosheets with ultrahigh conductivity for stamp-transferrable electrodes. J Am Chem Soc 135:5144–5151
32. Varma SJ, Kumar J, Liu Y, Layne K, Wu J, Liang C, Nakanishi Y, Aliyan A, Yang W, Ajayan PM, Thomas J (2017) 2D TiS_2 layers: a superior nonlinear optical limiting material. Adv Opt Mater 5:1700713
33. Lucovsky G, White RM, Benda JA, Revelli JF (1973) Infrared-reflectance spectra of layered group-iv and group-vi transition-metal dichalcogenides. Phys Rev B 7:3859–3870
34. Sandoval S, Chen X, Irwin J (1992) Raman spectra of Ag_xTiS_2 and lattice dynamics of TiS_2. Phys Rev B 45:14347–14353
35. Dolui K, Sanvito S (2016) Dimensionality-driven phonon softening and incipient charge density wave instability in TiS_2. EPL (Europhys Lett) 115:47001
36. Mukherjee S, Maiti R, Midya A, Das S, Ray SK (2015) Tunable direct bandgap optical transitions in MoS_2 nanocrystals for photonic devices. ACS Photonics 2:760–768
37. Sharma S, Bhagat S, Singh J, Singh RC, Sharma S (2017) Excitation-dependent photoluminescence from WS_2 nanostructures synthesized via top-down approach. J Mater Sci 52:11326–11336
38. Liu Y, O'Claus R (1997) Blue light emitting nanosized TiO_2 colloids. J Am Chem Soc 119:5273–5274
39. Mainwaring DE, Let AL, Rix C, Murugaraj P (2006) Titanium sulphide nanoclusters formed within inverse micelles. Solid State Commun 140:355–358
40. Sharma S, Singh J, Bhagat S, Singh M, Sharma S (2018) Size-tunable photoluminescence from WS_2 nanostructures. Mater Res Express 5:045047
41. Cunningham G, Lotya M, Cucinotta CS, Sanvito S, Bergin SD, Menzel R, Shaffer MSP, Coleman JN (2012) Solvent exfoliation of transition metal dichalcogenides: Dispersibility of exfoliated nanosheets varies only weakly between compounds. ACS Nano 6:3468–3480
42. Zuruzi AS, Kolmakov A, MacDonald NC, Moscovits M (2006) Highly sensitive gas sensor based on integrated titania nanosponge arrays. Appl Phys Lett 88:102904
43. Yue Q, Shao Z, Chang S, Li J (2013) Adsorption of gas molecules on monolayer MoS2 and effect of applied electric field. Nanoscale Res Lett 8:425
44. Zhou CJ, Yang WH, Wu YP, Lin W, Zhu HL (2015) Theoretical study of the interaction of electron donor and acceptor molecules with monolayer WS_2. J Phys D 48:285303
45. Singh J, Sharma S, Sharma S, Singh RC (2020) Effect of tungsten doping on structural and optical properties of rutile TiO_2 and band gap narrowing. Optik 182:538–547